Nanoscale Research Letters
a SpringerOpen Journal

NANO EXPRESS Open Access

First-principles study on transition metal-doped anatase TiO_2

Yaqin Wang[1], Ruirui Zhang[1], Jianbao Li[1], Liangliang Li[2] and Shiwei Lin[1*]

Abstract

The electronic structures, formation energies, and band edge positions of anatase TiO_2 doped with transition metals have been analyzed by *ab initio* band calculations based on the density functional theory with the planewave ultrasoft pseudopotential method. The model structures of transition metal-doped TiO_2 were constructed by using the 24-atom $2 \times 1 \times 1$ supercell of anatase TiO_2 with one Ti atom replaced by a transition metal atom. The results indicate that most transition metal doping can narrow the band gap of TiO_2, lead to the improvement in the photoreactivity of TiO_2, and simultaneously maintain strong redox potential. Under O-rich growth condition, the preparation of Co-, Cr-, and Ni-doped TiO_2 becomes relatively easy in the experiment due to their negative impurity formation energies, which suggests that these doping systems are easy to obtain and with good stability. The theoretical calculations could provide meaningful guides to develop more active photocatalysts with visible light response.

Keywords: First principles; Transition metal-doped TiO_2; Electronic structure; Formation energy; Band edge position

Background

The discovery of water photolysis on a TiO_2 electrode by Fujishima and Honda in 1972 [1] has been recognized as a landmark event. Since then, TiO_2 has attracted extensive attention as an ideal photocatalytic material because of its excellent properties such as high activity, good stability, nontoxicity and low cost. Thus, it has been widely used in the fields of renewable energy and ecological environmental protection [2-4]. However, as a wide band gap oxide semiconductor ($E_g = 3.23$ eV), anatase TiO_2 can only show photocatalytic activity under UV light irradiation ($\lambda < 387.5$ nm) that accounts for only a small portion of solar energy (approximately 5%), in contrast to visible light for a major part of solar energy (approximately 45%). Therefore, how to effectively utilize sunlight is the most challenging subject for the extensive application of TiO_2 as a photocatalyst. In the past decades, many efforts have been devoted to extending the spectral response of TiO_2 to visible light, including energy band modulation by doping with elements [5-11], the construction of heterojunctions by combining TiO_2 with metals such as Pt or Pd [12,13] and other semiconductors (such as MnO_2 [14], RuO_2 [15], and WO_3 [16]), and the addition of quantum dots [17] or dyes [18] on the surface of TiO_2 for better light sensitization.

Because of the unique *d* electronic configuration and spectral characteristics of transition metals, transition metal doping is one of the most effective approaches to extend the absorption edge of TiO_2 to visible light region, which either inserts a new band into the original band gap or modifies the conduction band (CB) or valence band (VB), improving the photocatalytic activity of TiO_2 to some degree [19-24]. For example, Umebayashi et al. [5] showed that the localized energy level due to Co doping was sufficiently low to lie at the top of the valence band, while the dopants such as V, Mn, Fe, Cr, and Ni produced the mid-gap states. Yu et al. [21] reported that the density functional theory (DFT) calculation further confirmed the red shift of absorption edges and the narrowing of the band gap of Fe-TiO_2 nanorods. Hou et al. [22] showed that new occupied bands were found in the band gap of Ag-doped anatase TiO_2. The formation of these new bands results from the hybridization of Ag 4*d* and Ti 3*d* states, and they were supposed to contribute to visible light absorption. Guo and Du [23] showed that Cu could lead to the enhancement of *d* states near the uppermost part of the

* Correspondence: linsw@hainu.edu.cn
[1]Key Laboratory of Ministry of Education for Advanced Materials in Tropical Island Resources, School of Materials and Chemical Engineering, Hainan University, Haikou 570228, People's Republic of China
Full list of author information is available at the end of the article

valence band of TiO_2 and the Ag or Au doping caused some new electronic states in the band gap.

Even though the effects of the transition metal-doped TiO_2 have been investigated frequently, it remains difficult to make direct comparisons and draw conclusions due to the various experimental conditions and different methods for sample preparation and photoreactivity testing. At the same time, because of the lack of the detailed information about the effects of metal doping on crystal structures and electronic structures, there is still much dispute about these issues. In comparison with the experimental investigation, the theoretical analysis by computer simulation can be a proper method to clarify the effects of transition metal doping in detail.

In order to systematically investigate the influence of transition metal doping into anatase TiO_2, we adopted the planewave ultrasoft pseudopotential method within the framework of density functional theory (DFT) to calculate the electronic structures, formation energies, and band edge positions of supercells, in which a Ti atom was substituted by a transition metal atom. Considering the accessibility of the doping metals, the 3*d* transition metal atoms (*M* = V, Cr, Mn, Fe, Co, Ni, Cu, and Zn) and the 4*d* transition metal atoms (*M* = Y, Zr, Nb, Mo, and Ag) were studied in the present work. Moreover, the present calculation results were compared with the experimental results reported in the literatures. The conclusions are important to understand the reactive mechanism and optimize the performance of TiO_2 photocatalysts that are active under visible light irradiation.

Methods

The electronic structures of the transition metal-doped TiO_2 were studied using first-principles calculation with the supercell approach. The unit cell of TiO_2 in the anatase structure and the $2 \times 1 \times 1$ supercell model considered in this study are shown in Figure 1a,b. Anatase TiO_2 has a tetragonal structure (space group, $I4_1/amd$), which contains four titanium atoms and eight oxygen atoms in a unit cell. Our model consists of two unit cells stacked along the *a*-axes, where one Ti atom was substituted by a 3*d* transition metal atom (*M* = V, Cr, Mn, Fe, Co, Ni, Cu, and Zn) or a 4*d* transition metal atom (*M* = Y, Zr, Nb, Mo, and Ag). The atomic percentage of the impurity was 4.17 at.%.

DFT calculations [25] were carried out using Cambridge Sequential Total Energy Package (CASTEP, Accelrys Company, San Diego, CA, USA) [26,27], with the planewave ultrasoft pseudopotential approach. Our geometry optimizations employed a local density approximation (LDA) exchange-correlation functional, while the Perdew-Burke-Ernzerh (PBE) of the generalized gradient approximation (GGA) was chosen to perform calculations to obtain the electronic structures and accurate formation energies. In these calculations, the cutoff energy of the planewave basis set was 380 eV. The Monkhorst-Pack scheme k-point grid sampling was set as $5 \times 5 \times 2$ for the irreducible Brillouin zone. The Pulay density mixing method was used in the computations of self-consistent field, and the self-consistent accuracy was set to the degree that every atomic energy converges to 2.0×10^{-6} eV. The force on every atom was smaller than 0.05 eV/nm. We calculated the total energy and electronic structures in the supercell under these conditions.

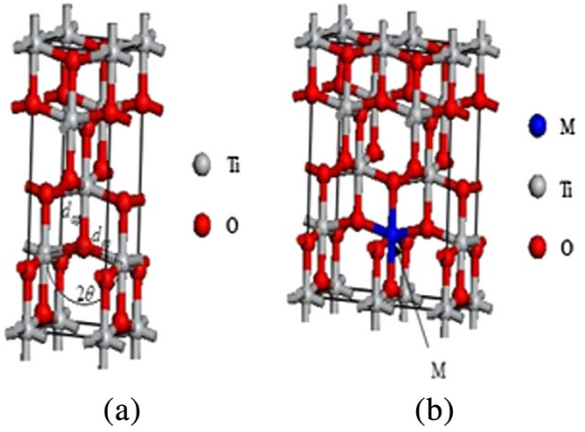

Figure 1 Models for calculation. (a) Unit cell of anatase TiO_2; **(b)** Structure of $2 \times 1 \times 1$ supercell model of transition metal-doped TiO_2. The gray spheres, the red spheres, and the blue sphere represent Ti atoms, O atoms, and transition metal atom, respectively.

Results and discussion

Structural optimization

The optimized structures of transition metal-doped anatase TiO_2 were calculated before the calculations of the electronic structures, which were performed to find the lattice parameters with the lowest energy. As shown in Table 1, the computational results for the structural parameters *a*, *c*, d_{ep}, d_{ap}, *c*/*a*, and 2θ are summarized together with the reported experimental values [28] and previous theoretical results [29]. The lattice parameters obtained in this work are in good agreement with the experimental data, and the deviation is less than 1.06% along

Table 1 Optimized structural parameters for anatase TiO_2 compared with experimental and previous theoretical results

	Experimental	This work		Literature [29]	
		Result	Deviation (%)	Result	Deviation (%)
a/Å	3.785	3.745	−1.06	3.692	−2.46
c/Å	9.514	9.466	−0.50	9.471	−0.45
d_{ep}/Å	1.934	1.914	−1.03	1.893	−2.12
d_{ap}/Å	1.978	1.969	−0.46	1.948	−1.52
c/*a*	2.513	2.528	0.56	2.566	+2.11

the *a*-axis or 0.5% along the *c*-axis. In comparison with the previous theoretical results reported in [29], our calculation results are more accurate, which verifies that the calculating method and models in this work are reliable and the calculated results are authentic.

Electronic structure

In order to conveniently investigate the electronic structures of transition metal-doped anatase TiO_2, we set the same k-points mesh to sample the first Brillouin zone for pure and transition metal-doped models. The calculated band gap of pure anatase TiO_2 is 2.21 eV as shown in Figure 2. The conduction band minimum (CBM) is located at G, while the valence band maximum (VBM) is located near *X*. So, the anatase TiO_2 can be considered as an indirect band gap semiconductor. The value of band gap is consistent with the reported results [29], but is underestimated compared with the experimental value (E_g = 3.23 eV), due to the limitation of DFT: the discontinuity in the exchange correlation potential is not taken into account within the framework of DFT. However, our discussions about energy gap will not be affected because only the relative energy changes are of concern.

The total density of states (TDOS) and partial density of states (PDOS) of transition metal-doped anatase TiO_2 in comparison with those of pure anatase TiO_2 are shown in Figures 3 and 4, which are treated by Gaussian broadening. The band gap is defined as the separation between the VBM and CBM. The TDOS shape of transition metal-doped TiO_2 becomes broader than that of pure TiO_2, which indicates that the electronic nonlocality is more obvious, owing to the reduction of crystal symmetry [19]. The transition metal 3*d* or 4*d* states are somewhat delocalized, which contributes to the formation of impurity energy levels (IELs) by hybridizing with O 2*p* states or Ti 3*d* states. Such hybrid effect may form energy levels in the band gap or hybrid with CBM/VBM, providing trapping

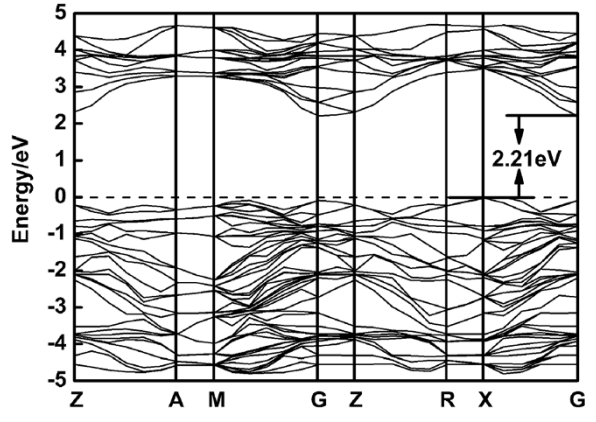

Figure 2 Calculated band structure of pure TiO_2.

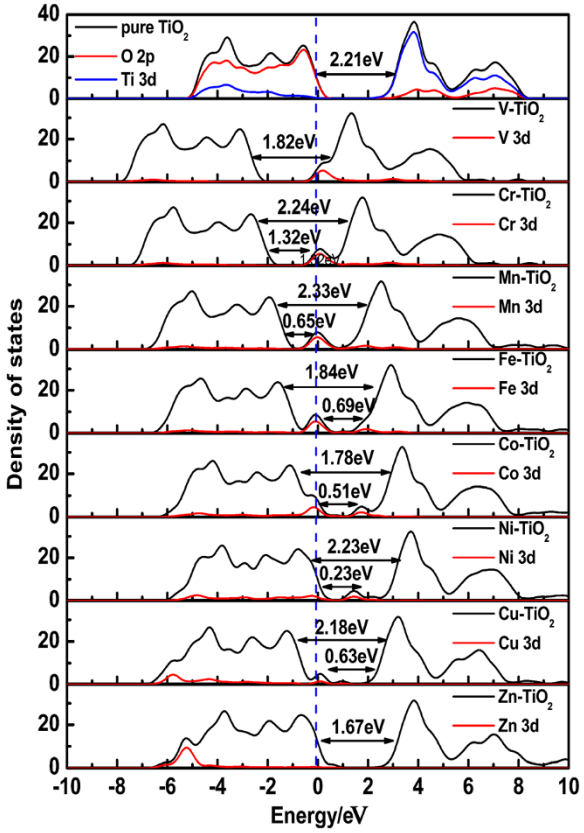

Figure 3 The TDOS and PDOS of the 3*d* transition metal-doped TiO_2 compared with pure TiO_2. Black solid lines: TDOS, and red solid lines: impurity's 3*d* states. The blue dashed line represents the position of the Fermi level.

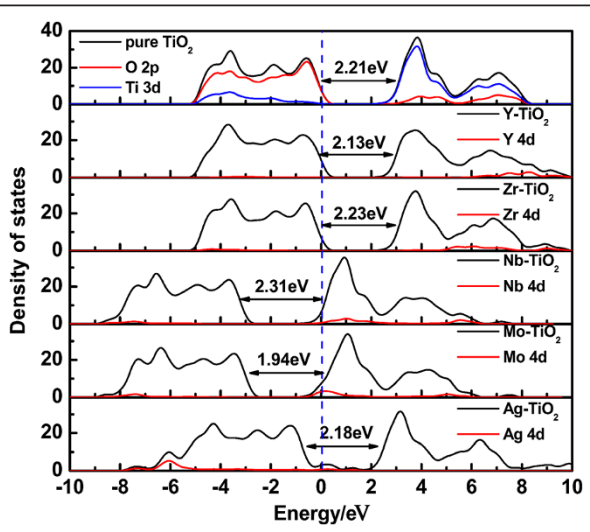

Figure 4 The TDOS and PDOS of the 4*d* transition metal-doped TiO_2 compared with pure TiO_2. Black solid lines: TDOS, and red solid lines: impurity's 4*d* states. The blue dashed line represents the position of the Fermi level.

potential well for electrons and holes. It gives a contribution to separation of photogenerated electron–hole pairs, as well as in favor of the migration of photoexcited carriers and the process of photocatalysis.

For TiO_2 doped with V, Cr, Mn, Fe, Co, Ni, Cu, Zn, Y, Zr, Nb, Mo, and Ag, considering the underestimation of the calculations, the band gaps of the transition metal-doped anatase TiO_2 are corrected by scissors operator. Scissors operator is used for a purpose as correction to the band gap, which has a clear separation between the CB and VB. For these calculations, the scissors operator is set at 1.02 eV, accounting for the difference between the experimental band gap (3.23 eV) and the calculated band gap (2.21 eV) for pure anatase TiO_2. Then, the band gaps of TiO_2 doped with V, Cr, Mn, Fe, Co, Ni, Cu, Zn, Y, Zr, Nb, Mo, and Ag, are determined as 2.84, 3.26, 3.35, 2.86, 2.80, 3.25, 3.20, 2.69, 3.15, 3.25, 3.33, 2.96, and 3.20 eV, respectively. It should be noted that the band gap of transition metal-doped TiO_2 is not related to the band gap between the Ti t_{2g} (d_{xy}, d_{xz}, d_{yz}) and e_g (d_{z^2}, $d_{x^2-y^2}$) bands, but to the energy separation between the O 2*p* and the Ti t_{2g} bands of TiO_2 that is modified by doping atoms.

In comparison with pure TiO_2, the calculation results of the electronic structures of Ti_7MO_{16} can be classified into six groups according to the position of the IELs in Figures 3 and 4: (1) Ti_7VO_{16} and Ti_7MoO_{16}; (2) Ti_7CrO_{16}; (3) Ti_7MnO_{16}, Ti_7FeO_{16}, Ti_7CoO_{16}, Ti_7NiO_{16}, and Ti_7AgO_{16}; (4) Ti_7CuO_{16}; (5) Ti_7ZnO_{16} and Ti_7YO_{16}; and (6) Ti_7ZrO_{16} and Ti_7NbO_{16}.

- Ti_7VO_{16} and Ti_7MoO_{16}. The IELs are located at the bottom of the CB and mixed with the Ti 3*d* states to form a new CBM, which leads to an obvious band gap narrowing. The position of the IELs might result in a red shift, which gives an explanation of the experimental optical absorption spectra of V-doped TiO_2 [30]. The positions of the IELs in the Mo-doped system in Figure 4 are similar to those in V-doped TiO_2, which may also result in red shift of absorption spectra in experiments.
- Ti_7CrO_{16}. The IELs are located below the CBM with a small distance. For Cr-doped TiO_2, the IELs act as a shallow donor, and their occurrence is mainly due to the Cr 3*d* states that lie at the bottom of CB as shown in Figure 3. As the E_F crosses it, it is partially filled with electrons at the ground state. In this case, the optical transitions are expected to be two transitions. One is the acceptor transition from the VBM to the IELs. The other is a donor transition from the IELs into the CBM. Meanwhile, VB holes and CB electrons appear. The former contributes to the anodic photocurrent, and the latter contributes to the cathodic photocurrent under visible light. Then, the Cr-doped system can serve as a remarkably better photocatalyst.
- Ti_7MnO_{16}, Ti_7FeO_{16}, Ti_7CoO_{16}, Ti_7NiO_{16}, and Ti_7AgO_{16}. The IELs occur in the middle of the band gap, namely the intermediate level. They may reduce the energy required for electron transition, lower the threshold of photoexcitation, and thus expand the optical absorption spectrum without reducing the energy of electrons or holes. The electrons in the VB can be excited to the IELs and then subsequently excited to the CB by the visible light irradiation. So, IELs are beneficial for extending the sensitive light wavelength. The result gives a good explanation of the red shift [31-34]. However, for these kinds of IELs, high impurity doping concentration might form a recombination center for photoexcited electron–hole pairs and results in a decrease in the quantum yield for the photocatalytic reactions [21]. Therefore, we must control the doping concentration to avoid them to act as the recombination center of photo-generated electrons and holes.
- Ti_7CuO_{16}. The IELs are located above the VB and partially overlap with the VBM. These kinds of IELs could act as trap centers for photoexcited holes, which can also reduce the recombination rate of charge carriers [10]. The holes generated in the VB produce an anodic photocurrent. Because the Cu t_{2g} level is close to the VB, the holes easily overlap in highly impure media [5].
- Ti_7ZnO_{16} and Ti_7YO_{16}. The IELs are located at the top of the VB and completely mixed with the O 2*p* states to form a new VBM (seen in Figures 3, 4, and 5). The band gaps of Zn- and Y-doped anatase TiO_2 are narrowed to 2.69 and 3.15 eV, respectively, and smaller than that of pure TiO_2, which is consistent with the experimental data on the red shift of the absorption edge [35,36].
- Ti_7ZrO_{16}, Ti_7NbO_{16}. The IELs are not situated at band gap. The electronic structure of Zr-doped TiO_2 exhibits similar to that of pure TiO_2. Therefore, we can infer that the t_{2g} level due to Zr does not contribute to the photo-response. Similarly, the band gap of Nb-doped anatase TiO_2 is larger than that of undoped TiO_2 by 0.09 eV, which may result in a blue shift of the absorption edge.

Formation energy

We analyzed the relative difficulty for different transition metal doping into anatase TiO_2 using impurity formation energies, which is a widely accepted method. First-principles calculation for the relative stability of metal-doped TiO_2 can help us understand the formation of the doped structures and provide useful guidance to

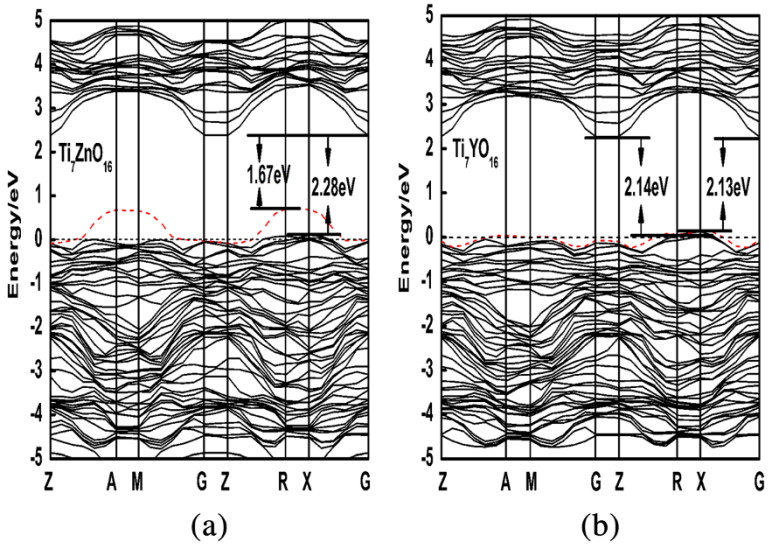

Figure 5 Calculated band structure. (a) Zn-doped anatase TiO_2; **(b)** Y-doped anatase TiO_2.

prepare samples. In this section, to investigate the relative difficulty for single doping atom to incorporate into the lattice, we calculated the impurity formation energy E_{form} (M^{q}) as follows [9,37]:

$$E_{\text{form}}(\text{M}^{\text{q}}) = E_{\text{total}}(\text{M}^{\text{q}}) - E_{\text{total}}(\text{pure}) - \sum_{\text{i}} n_{\text{i}}\mu_{\text{i}} + q(E_{\text{F}} + E_{\text{v}} + \Delta V), \quad (1)$$

where $E_{\text{total}}(M^{\text{q}})$ is the total energy of metal-doped TiO_2, and E_{total}(pure) is the total energy of the pure TiO_2. n_{i} is the number of atoms from species M (=Ti) being removed from a defect-free cell to its respective reservoir with chemical potential μ_{i}. The chemical potential reflects the availability or the elemental partial pressure of each element. E_{F} is the reference level according to the valence band level (E_{v}), and ΔV is often simplified as zero. In the present work, the transition metal M substitutes Ti in the calculated models, and the impurity formation energy $E_{\text{form}}(M)$ could thus be defined using the following formula [38,39]:

$$E_{\text{form}}(M) = E_{\text{total}}(M) - E_{\text{total}}(\text{pure}) - \mu_{\text{M}} + \mu_{\text{Ti}}, \quad (2)$$

where μ_{M} is the chemical potential of the doping metal. μ_{Ti} is the chemical potential of Ti and depends on the experimental growth condition, which can be Ti-rich or O-rich (or any case in between). Under Ti-rich condition, the Ti chemical potential can be assumed in thermodynamic equilibrium with the energy of bulk Ti, while the O chemical potential can be obtained by the growth condition:

$$E_{\text{TiO}_2} = \mu_{\text{Ti}} + 2\mu_{\text{o}}. \quad (3)$$

Under O-rich condition, the chemical potential of O can be calculated from the ground state energy of O_2 molecule, while the chemical potential of Ti is fixed by Equation (3). The chemical potentials for metals (μ_{M}) are fixed and calculated from the formula below [40,41]:

$$\mu_{\text{M}} = \left(\mu_{\text{M}_{\text{m}}\text{O}_{\text{n}}} - n\mu_{\text{O}}\right)/m, \quad (4)$$

where $\mu_{\text{M}_{\text{m}}\text{O}_{\text{n}}}$ is the energy of the most stable oxide for doping atoms at room temperature.

The formation energies $E_{\text{form}}(M)$ for the 13 different metal-doped models of 24-atom supercell under O-rich condition are calculated and listed in Table 2. In terms of the formation energy, the transition metals that intend to substitute Ti are in the order of Mo < Zn < Ag < V < Y < Cu < Mn < Nb < Fe < Zr < Cr < Ni < Co under O-rich growth

Table 2 Impurity formation energies of 3*d* and 4*d* transition metal-doped TiO_2 supercells under O-rich condition

Metal doping system	$\mu_{\text{M}_{\text{m}}\text{O}_{\text{n}}}$/eV	μ_{M}/eV	E_{form}(M)/eV
V/TiO_2	−6,141.7221	−1,985.7396	1.5761
Cr/TiO_2	−6,247.8894	−2,472.8718	−0.3744
Mn/TiO_2	−1,526.5251	−658.4279	1.0589
Fe/TiO_2	−3,039.9476	−868.9009	0.4044
Co/TiO_2	−1,478.3064	−1,044.2578	−1.3011
Ni/TiO_2	−1,789.8414	−1,355.7928	−0.671
Cu/TiO_2	−1,782.5169	−1,348.4683	1.1586
Zn/TiO_2	−2,147.2478	−1,713.1992	2.082
Y/TiO_2	19,299.7106	−3,426.724	1.2848
Zr/TiO_2	−2,160.6581	−1,292.5609	0.294
Nb/TiO_2	−19,799.3096	−5,292.2674	0.4089
Mo/TiO_2	−3,248.3724	−1,946.2266	3.3946
Ag/TiO_2	−1,462.3681	−1,028.3195	1.77

condition. It is difficult to find the tendency of $E_{form}(M)$ with the increase in atomic number in each element period. The formation energies of substitutional Co, Ni, and Cr-doped models are negative and less than those of the models substituted by other transition metals under O-rich growth condition. This indicates that under O-rich growth condition, it is energetically more favorable to replace Ti with Co, Ni, and Cr than other metals. The synthesis of the Co-, Ni-, and Cr-doped anatase TiO_2 system with a higher doping level would be relatively easy in the experiment because a much smaller formation energy is required. This might be because the ionic radii of Cr^{3+}, Co^{3+}, and Ni^{2+} are close to Ti^{4+}. Presumptively, we suggest that the impurity formation energy is sensitive to the ionic radius of impurity. The results can provide some useful guidance to prepare metal-doped TiO_2 and other oxide semiconductors.

To further investigate the influence of transition metal doping, we combine the band gap values and the formation energies of the transition metal-doped TiO_2 in Figure 6. This can provide important guidance for the experimentalists to prepare thermodynamically stable photocatalysts with visible light response. Under O-rich growth condition, anatase TiO_2 doped with various transition metals has different formation energies, where the formation energies of Cr-, Co-, and Ni-TiO_2 are negative. This suggests that such doping is an energetically favorable process. Considering the band gap narrowing effects only, we can find that the band gap is narrowed to 1.78 eV for Co doping, but broadened to 2.24 and 2.23 eV for Cr and Ni doping, respectively. However, TiO_2 doped with Cr, Co, and Ni, as well as Ag, Fe, Mn, and Cu, which are marked red in Figure 6 and form impurity energy levels in the band gap as shown in Figure 3, might improve the photocatalytic activity with a low doping concentration, but can act as the recombination center for the photo-generated electron–hole pairs with a high doping concentration and result in an unfavorable effect on the photocatalytic activity. In comparison, TiO_2 doped with V, Zn, Y, and Mo, as shown in Figure 6, possess narrower band gaps than pure TiO_2 with the IELs mixed with Ti 3*d* states or O 2*p* states. These doping systems result in red shift of absorption edge without forming a recombination center and could improve the photocatalytic activity well. Zr- and Nb-doped anatase TiO_2 do not form the IELs in the middle of the band gap, and even broaden the band gap, which might result in a blue shift. Furthermore, except for Cr-, Co-, and Ni-doped anatase TiO_2, the positive formation energies of other transition metal doping systems imply relative difficulty for fabrication in experiments.

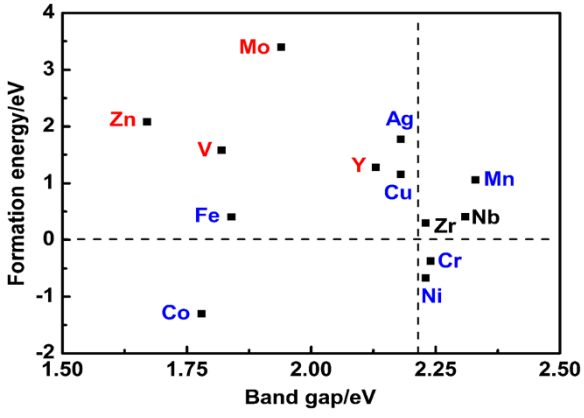

Figure 6 Relationship between the band gaps and formation energies of 3*d* and 4*d* transition metal-doped TiO_2. The elements colored in black are elements that do not form the impurity levels in the band gap. The elements colored in red are elements that form the impurity levels in the band gap but do not form the middle level. The elements colored in blue are elements that occur in the impurity levels in the band gap and form the middle levels. The horizontal dashed line indicates 0 eV, and the vertical dashed line represents the calculated band gap of pure TiO_2 (2.21 eV).

Band edge position

The band edge position of a semiconductor as well as the redox potentials of the adsorbate governs the ability of a semiconductor to undergo photoexcited electron transfer to adsorb substances on its surface [39]. The relevant potential level of the donor thermodynamically needs to be more negative than the VB edge position of the semiconductor in order to donate an electron to the vacant hole. In addition, the potential level of the acceptor is required to be more positive than the CB potential of the semiconductor [42]. So, we calculated the band edge position of the semiconductor photocatalyst to understand the redox reactivity.

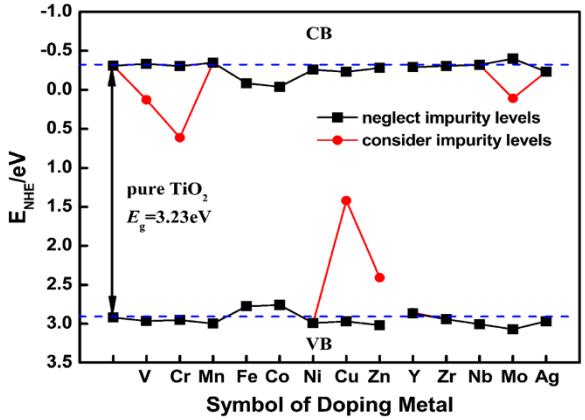

Figure 7 The calculated band edge positions of 3*d* and 4*d* transition metal-doped TiO_2. The black line is taken as the condition that neglects the impurity levels, and the red line represents the condition that considers the impurity levels. The black line with double arrow is the band gap energy of pure TiO_2 corrected by scissors operator. The blue dashed lines represent the CB/VB edge potential of pure TiO_2.

The CB and VB edge positions of a semiconductor can be expressed empirically by the following formula [43-46]:

$$E_{CB} = X - E^{e} - \frac{1}{2}E_{g}$$
$$E_{VB} = E_{g} + E_{CB}, \quad (5)$$

where E_{CB} is the CB edge potential, and E_{VB} is the VB edge potential. X is the geometric mean of the electronegativity of the constituent atoms [47,48], E^{e} is the energy of free electrons on the hydrogen scale (approximately 4.5 eV), and E_{g} is the band gap energy of the semiconductor corrected by scissors operator. The CB edge potential of TiO_2 is −0.31 eV with respect to the normal hydrogen electrode (NHE), while the VB edge potential is determined to be 2.92 eV. This result is consistent with the band edge position of TiO_2. The band edge positions of TiO_2 doped with the transition metals relative to that of pure TiO_2 are summarized in Figure 7, and the data show that most transition metal-doped anatase TiO_2 can maintain the strong redox potentials. Moreover, in terms of TiO_2 doped with V, Mn, Nb, and Mo, the CB edges are slightly shifted upward and the VB edges are slightly shifted downward as compared with those of pure TiO_2. This means that V, Mn, Nb, and Mo doping could even enhance the redox potentials of TiO_2.

Conclusions

Transition metal-doped TiO_2 has been studied using first-principles density functional theory. The calculated results show that owing to the formation of the impurity energy levels, which is mainly hybridized by 3*d* or 4*d* states of impurities with O 2*p* states or Ti 3*d* states, the response region in spectra could be extended to the visible light region. The position of the impurity energy levels in the band gap determines the effects of metal doping on the photocatalytic performance of TiO_2. Most transition metal doping could narrow the band gap of TiO_2, lead to the improvement of the photoreactivity of TiO_2, and simultaneously maintain strong redox potential. Under O-rich growth condition, formation energies of anatase TiO_2 doped with various metals are different. Particularly, the formation energies of TiO_2 doped with Cr, Co, and Ni are found to be negative, showing that it is energetically more favorable to substitute Co, Ni, or Cr to a Ti site than other metals. These doping systems can be easily obtained and with good stability.

Theoretical research on transition metal-doped TiO_2 is of great importance to develop the photocatalytic applications. First-principles calculation of doped TiO_2 is still an ongoing subject, and a few challenging problems require further investigation in an urgent demand. One is the influence of the transition metal doping on the phase transition of TiO_2 from anatase to rutile. A theoretical understanding on its mechanism will be useful to optimize the performance of TiO_2 in photocatalytic and other applications. Another one is the question about using the virtual crystal approximation method to calculate the doping system for very low concentration, which can cut down the calculation time. With the solution of these problems, one could provide more accurate theoretical models to simulate the practical doping approaches which could lead to important implications in the optimization of the performance of transition metal-doped TiO_2 photocatalysts.

Competing interests

The authors declare that they have no competing interests.

Authors' contributions

SW conceived the idea and designed the calculated model. YQ and RR carried out the calculations and data analysis. JB and LL participated in the design of the study and helped in drafting the manuscript. All authors read and approved the final manuscript.

Acknowledgements

This work was supported by the National Nature Science Foundation of China (51162007 and 51202050), Hainan Natural Science Foundation (511110), and Tsinghua University Initiative Scientific Research Program.

Author details

[1]Key Laboratory of Ministry of Education for Advanced Materials in Tropical Island Resources, School of Materials and Chemical Engineering, Hainan University, Haikou 570228, People's Republic of China. [2]Department of Materials Science and Engineering, Key Laboratory of Advanced Materials, Tsinghua University, Beijing 100084, People's Republic of China.

Received: 1 November 2013 Accepted: 5 December 2013
Published: 28 January 2014

References

1. Fujishima A, Honda K: **Electrochemical photolysis of water at a semiconductor electrode.** *Nature* 1972, **23:**37–38.
2. Yang K, Dai Y, Huang B, Han S: **Theoretical study of N-doped TiO_2 rutile crystals.** *J Phys Chem B* 2006, **110:**24011–24014.
3. Li SP, Lin SW, Liao JJ, Pan NQ, Li DH, Li JB: **Nitrogen-doped TiO_2 nanotube arrays with enhanced photoelectrochemical property.** *Int J Photoenergy* 2012, **2012:**794207.
4. Luo W, Yu T, Wang Y, Li Z, Ye J, Zou Z: **Enhanced photocurrent-voltage characteristics of WO_3/Fe_2O_3 nano-electrodes.** *J Phys D Appl Phys* 2007, **40:**1091.
5. Umebayashi T, Yamaki T, Itoh H, Asai K: **Analysis of electronic structures of 3d transition metal-doped TiO_2 based on band calculations.** *J Phys Chem Solids* 2002, **63:**1909–1920.
6. Chen X, Burda C: **The electronic origin of the visible-light absorption properties of C–, N- and S-doped TiO_2 nanomaterials.** *J Am Chem Soc* 2008, **130:**5018–5019.
7. Xu J, Wang J, Lin Y, Liu X, Lu Z, Lu Z, Lv L, Zhang F, Du Y: **Effect of annealing ambient on the ferromagnetism of Mn-doped anatase TiO_2 films.** *J Phys D Appl Phys* 2007, **40:**4757.
8. Shankar K, Tep KC, Mor GK, Grimes CA: **An electrochemical strategy to incorporate nitrogen in nanostructured TiO_2 thin films.** *J Phys D Appl Phys* 2006, **39:**2361.
9. Han X, Shao G: **Electronic properties of rutile TiO_2 with nonmetal dopants from first principles.** *J Phys Chem C* 2011, **116:**8274–8282.
10. Zhao Z, Liu Q: **Effects of lanthanide doping on electronic structures and optical properties of anatase TiO_2 from density functional theory calculations.** *J Phys D Appl Phys* 2008, **41:**085417.
11. De Angelis F, Fantacci S, Selloni A, Nazeeruddin MK, Grätzel M: **First-principles modeling of the adsorption geometry and electronic structure of Ru (II) dyes on extended TiO_2 substrates for dye-sensitized solar cell applications.** *J Phys Chem C* 2010, **114:**6054–6061.

12. Yoon KJ, Lee MH, Kim GH, Song SJ, Seok JY, Han S, Yoon JH, Kim KM, Hwang CS: **Memristive tri-stable resistive switching at ruptured conducting filaments of a Pt/TiO_2/Pt cell.** *Nanotechnol* 2012, **23:**185202.
13. Nishikawa M, Sakamoto H, Nosaka Y: **Reinvestigation of the photocatalytic reaction mechanism for Pt-complex-modified TiO_2 under visible light irradiation by means of ESR spectroscopy and chemiluminescence photometry.** *J Phys Chem A* 2012, **116:**9674–9679.
14. Xue M, Huang L, Wang JQ, Wang Y, Gao L, Zhu J, Zou ZG: **The direct synthesis of mesoporous structured MnO_2/TiO_2 nanocomposite: a novel visible-light active photocatalyst with large pore size.** *Nanotechnol* 2008, **19:**185604.
15. Ismail AA, Robben L, Bahnemann DW: **Study of the efficiency of UV and visible-light photocatalytic oxidation of methanol on mesoporous RuO_2-TiO_2 nanocomposites.** *Chem Phys* 2011, **12:**982–991.
16. Chainarong S, Wei X, Sikong L, Pavasupree S: **The effect of molar ratio of TiO_2/WO_3 nanocomposites on visible light prepared by hydrothermal method.** *Adv Mater Res* 2012, **488:**572–577.
17. Peng H, Li J, Li SS, Xia JB: **First-principles study on rutile TiO_2 quantum dots.** *J Phys Chem C* 2008, **112:**13964–13969.
18. Hahlin M, Johansson EMJ, Plogmaker S, Odelius M, Hagberg DP, Sun L, Siegbahn H, Rensmo H: **Electronic and molecular structures of organic dye/TiO_2 interfaces for solar cell applications: a core level photoelectron spectroscopy study.** *Chem Phys Phys Chem* 2010, **12:**1507–1517.
19. Shao G: **Electronic structures of manganese-doped rutile TiO_2 from first principles.** *J Phys Chem C* 2008, **112:**18677–18685.
20. Valentin CD, Pacchioni G, Onishi H, Kudo A: **Cr/Sb co-doped TiO_2 from first principles calculations.** *Chem Phys Lett* 2009, **469:**166–171.
21. Yu J, Xiang Q, Zhou M: **Preparation, characterization and visible-light-driven photocatalytic activity of Fe-doped titania nanorods and first-principles study for electronic structures.** *Appl Catal B Environ* 2009, **90:**595–602.
22. Hou XG, Liu AD, Huang MD, Liao B, Wu XL: **First-principles band calculations on electronic structures of Ag-doped rutile and anatase TiO_2.** *Chin Phys Lett* 2009, **26:**077106.
23. Guo M, Du J: **First-principles study of electronic structures and optical properties of Cu, Ag, and Au-doped anatase TiO_2.** *Physica B* 2012, **407:**1003–1007.
24. Zhang LK, Wu B, Wang M, Chen L, Ye GX, Chen T, Liu HL, Huang CR, Li JL: **Crystal, electronic and magnetic structure of Co and Ag doped rutile TiO_2 from first-principles calculations.** *Adv Mater Res* 2012, **399:**1789–1792.
25. Ferreira LG, Marques M, Teles LK: **Approximation to density functional theory for the calculation of band gaps of semiconductors.** *Phys Rev B* 2008, **78:**125116.
26. Clark SJ, Segall MD, Pickard CJ, Hasnip PJ, Probert MIJ, Refson K, Payne MC: **First principles methods using CASTEP.** *Z Kristallogr* 2005, **220:**567–570.
27. Segall M, Lindan PJD, Probert M, Pickard C, Hasnip P, Clark S, Payne M: **First-principles simulation: ideas, illustrations and the CASTEP code.** *J Phys Condens Matter* 2002, **14:**2717.
28. Burdett JK, Hughbanks T, Miller GJ, Richardson JW Jr, Smith JV: **Structural-electronic relationships in inorganic solids: powder neutron diffraction studies of the rutile and anatase polymorphs of titanium dioxide at 15 and 295 K.** *J Am Chem Soc* 1987, **109:**3639–3646.
29. Asahi R, Taga Y, Mannstadt W, Freeman A: **Electronic and optical properties of anatase TiO_2.** *Phys Rev B* 2000, **61:**7459.
30. Choi W, Termin A, Hoffmann MR: **The role of metal ion dopants in quantum-sized TiO_2: correlation between photoreactivity and charge carrier recombination dynamics.** *J Phys Chem B* 1994, **98:**13669–13679.
31. Bouaine A, Schmerber G, Ihiawakrim D, Derory A: **Structural, optical, and magnetic properties of polycrystalline Co-doped TiO_2 synthesized by solid-state method.** *Mater Sci Eng* 2012, **177:**1618–1622.
32. Lu L, Xia X, Luo JK, Shao G: **Mn-doped TiO_2 thin films with significantly improved optical and electrical properties.** *J Phys D Appl Phys* 2012, **45:**485102.
33. Singh D, Singh N, Sharma SD, Kant C, Sharma CP, Pandey RR, Saini KK: **Bandgap modification of TiO_2 sol–gel films by Fe and Ni doping.** *J Sol–Gel Sci Technol* 2011, **58:**269–276.
34. Su R, Bechstein R, Kibsgaard J, Vang RT, Besenbacher F: **High-quality Fe-doped TiO_2 films with superior visible-light performance.** *J Mater Chem* 2012, **22:**23755–23758.
35. Wang KP, Teng H: **Zinc-doping in TiO_2 films to enhance electron transport in dye-sensitized solar cells under low-intensity illumination.** *Chem Phys Phys Chem* 2009, **11:**9489–9496.
36. Zhang H, Tan K, Zheng H, Gu Y, Zhang W: **Preparation, characterization and photocatalytic activity of TiO_2 codoped with yttrium and nitrogen.** *Mater Chem Phys* 2011, **125:**156–160.
37. Van de Walle CG, Neugebauer J: **First-principles calculations for defects and impurities: applications to III-nitrides.** *J Appl Phys* 2004, **95:**3851.
38. Cui X, Medvedeva J, Delley B, Freeman A, Newman N, Stampfl C: **Role of embedded clustering in dilute magnetic semiconductors: Cr doped GaN.** *Phys Rev Lett* 2005, **95:**256404.
39. Zhao Z, Liu Q: **Designed highly effective photocatalyst of anatase TiO_2 codoped with nitrogen and vanadium under visible-light irradiation using first-principles.** *Catal Lett* 2008, **124:**111–117.
40. Long R, English NJ: **First-principles calculation of synergistic (N, P)-codoping effects on the visible-light photocatalytic activity of anatase TiO_2.** *J Phys Chem C* 2010, **114:**11984–11990.
41. Yang K, Dai Y, Huang B, Whangbo MH: **Density functional characterization of the band edges, the band gap states, and the preferred doping sites of halogen-doped TiO_2.** *Chem Mater* 2008, **20:**6528–6534.
42. Linsebigler AL, Lu G, Yates JT Jr: **Photocatalysis on TiO_2 surfaces: principles, mechanisms, and selected results.** *Chem Rev* 1995, **95:**735–758.
43. Zhao Z, Liu Q: **Mechanism of higher photocatalytic activity of anatase TiO_2 doped with nitrogen under visible-light irradiation from density functional theory calculation.** *J Phys D Appl Phys* 2008, **41:**025105.
44. Xu Y, Schoonen MAA: **The absolute energy positions of conduction and valence bands of selected semiconducting minerals.** *Am Mineral* 2000, **85:**543–556.
45. Kim YI, Atherton SJ, Brigham ES, Mallouk TE: **Sensitized layered metal oxide semiconductor particles for photochemical hydrogen evolution from nonsacrificial electron donors.** *J Phys Chem* 1993, **97:**11802–11810.
46. Tang J, Ye J: **Photocatalytic and photophysical properties of visible-light-driven photocatalyst $ZnBi_{12}O_{20}$.** *Chem Phys Lett* 2005, **410:**104–107.
47. Putz MV, Russo N, Sicilia E: **About the Mulliken electronegativity in DFT.** *Theor Chem Acc* 2005, **114:**38–45.
48. Frese KW: **Simple method for estimating energy levels of solids.** *J Vac Sci Technol* 1979, **16:**1042–1044.

doi:10.1186/1556-276X-9-46
Cite this article as: Wang *et al.*: First-principles study on transition metal-doped anatase TiO_2. *Nanoscale Research Letters* 2014 **9**:46.